Lifetime effects in low-stage intercalated graphite systems

Kenneth W. -K. Shung
Solid State Division, Oak Ridge National Laboratory, Oak Ridge, Tennessee 37831
and Department of Physics, University of Tennessee, Knoxville, Tennessee 37916
(Received 3 February 1986)

Based upon a superlattice model for graphite intercalated compounds (GIC's), we present in this paper a detailed calculation of the lifetime of a conduction electron in a stage-1, acceptor-type GIC. Both intraband and interband processes, as well as intervalley processes, are included in this calculation. We find that it is very important to include the dynamic screening in the scheme, because the Coulomb interaction can generate plasmons that provide an efficient way for electrons to decay. The calculated electronic lifetime is then applied to the examination of the broad edge structure found in optically induced interband transitions. There, only partial success is found, possibly because of inaccurate determination of the Fermi energy. Improvements of our present calculation are suggested.

I. INTRODUCTION

Recently, Hoffman and co-workers[1] carefully studied optical reflectance of acceptor-type graphite intercalation compounds (GIC's). By carrying out a Kramers-Kronig phase-shift analysis, they obtained the optical dielectric function $\epsilon(\omega)=\epsilon_1(\omega)+i\epsilon_2(\omega)$. This measured $\epsilon(\omega)$ was successfully interpreted in terms of the two-dimensional (2D) model of GIC's proposed by Blinowski *et al.*[2] However, the measured result has a broad interband transition edge at $\omega=2\epsilon_F$ (ϵ_F denotes the Fermi energy)—a profile not readily explained by the 2D model. In this work, we want to examine the lifetime effect on the edge structure. This problem will be made clearer below, after we outline the results from the calculations of Blinowski and coworkers.

In the 2D model, Blinowski *et al.* treat a stage-n compound as a collection of an infinite number of slabs, each of which contains n graphite layers that are confined by two intercalate layers. In this model, every graphite slab is equivalent to, but independent of, another; hence, one only needs to take one graphite slab to calculate the band structure. Let us confine ourselves to the $n=1$ case here, because stage-1 compounds have the simplest band structure and are believed to be well described by the 2D model.[2-4] The band structure of one graphite layer is calculated by a straightforward tight-binding method,[2] and main features from this calculation are shown in Fig. 1. Close to the hexagonal corners (U or U'), energy bands are linear in $k=|\mathbf{k}|$ ($\mathbf{k}$ being measured from one of the corners):

$$\epsilon_k^{c,v}=\pm v_F k \ , \tag{1}$$

where $v_F=\frac{3}{2}\gamma_0 b$; $\gamma_0=2.4$ eV and $b=1.42$ Å; the latter is the distance of neighboring carbon atoms.[2] We used the superscript c (v) to indicate that the electron is in the conduction (valence) band. We shall keep this practice, and when the superscript is missing from an energy expression, we mean its absolute value, e.g., $\epsilon_q=v_F q$. For acceptor-type GIC's, the valence band becomes partially vacant and the Fermi level is lowered from the degenerate U (or U') point into the valence band, as shown in the figure.

The optically induced interband transition ($v\rightarrow c$) is indicated by the upward arrow in Fig. 1. Clearly, the minimum energy required for the interband transition is $2\epsilon_F$ (with broadening effects neglected). Let us denote the part of the dielectric function from the interband transition by $\epsilon_{v\text{-}c}(\omega)$. From the 2D model, it was found[2] that ($\hbar=1$)

$$\mathrm{Im}\epsilon_{v\text{-}c}(\omega)=\frac{-e^2v_F^2}{\pi\omega I_c} \times\int_{\mathrm{BZ}} dk\frac{n_k^v}{\omega_k}\left[\frac{1}{\omega-\omega_k+i\eta}-\frac{1}{\omega+\omega_k+i\eta}\right], \tag{2}$$

where I_c is the distance between two adjacent graphite

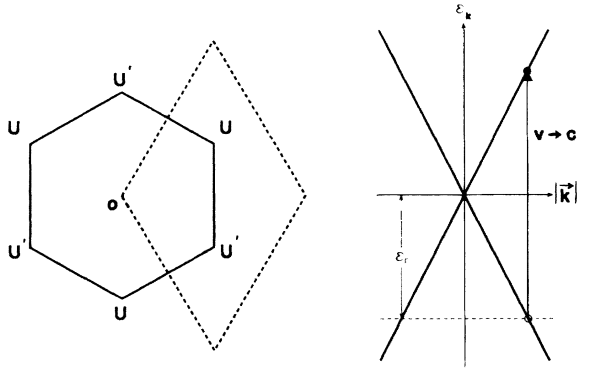

FIG. 1. Two alternative ways to choose the first Brillouin zone are shown on the left. The linear band structure in the vicinity of the symmetric point U (or U') is shown on the right. For acceptor-type GIC's, the Fermi energy is lowered from the degenerate point to a level within the valence band, as indicated in the figure. As a result, the optically induced interband transition (the upward arrow) has a minimum energy of $2\epsilon_F$.

layers ($I_c = 9.42$ Å),[1] $\omega_k = \varepsilon_k^c - \varepsilon_k^v = 2v_F k$, η is an infinitesimal positive number, n_k^v is the Fermi distribution function ($1 - n_k^c = 1$ for all k), and the integration is done over the Brillouin zone. Again, we used the superscripts v and c to indicate the band the electron is in. If the electron lifetime is neglected, Eq. (2) has a simple result,[2]

$$\mathrm{Im}\epsilon_{v\text{-}c}(\omega) = \frac{\pi e^2}{I_c \omega} \frac{1}{1 + e^{(2\varepsilon_F - \omega)/2k_B T}} \quad (\omega > 0) , \tag{3}$$

where T is the laboratory temperature. When T is not too high, this result suggests a sharp edge at $\omega = 2\varepsilon_F$. However, it was found[1,2] that this expression could not describe the measured interband transition edge unless a very high effective temperature ~ 1000 K is used, while in fact $T = 300$ K. Blinowski *et al.* attributed this large broadening effect to scattering associated with the interband transitions, although they did not provide details. Hoffman and co-workers, using a modified 2D model, have considered the broadening effects due to the c-axis dispersion.[5] There, extra parameters are needed to explain the experimental data.

Our object in this work is to examine the broadening effect due to the inelastic Coulomb scattering experienced by the excited electron, which is now in the conduction band. The width of the hole left in the valence band is neglected because of the phase-space restriction. We can also neglect phonons in this problem since the broadening has been shown to be temperature insensitive.[5] In the calculation of the electron lifetime, it is important to use a screened potential for the Coulomb interaction.[6] An appropriate dielectric function that describes the screening mechanism for low-stage GIC's has been evaluated by the author in a separate paper.[7] In that work, the dielectric function is calculated according to a superlattice model, in which (a) a GIC is a system composed of an infinite number of identical graphite layers, (b) each graphite layer is described by the 2D model of Blinowski *et al.*, (c) electron tunneling between different layers is neglected, (d) electrons on different layers can interact via the Coulomb interaction, and (e) the only effect due to intercalants is restricted to the determination of the Fermi energy. Based on this model, the dielectric function has been analytically evaluated, and can thus be applied here directly. More discussions on this superlattice model can be found in Ref. 7, and a summary of the results from that work is given in the Appendix. Note that, by neglecting the interlayer tunneling, we can still use Eq. (2) to describe the optically induced interband transitions. The inclusion of the broadening effect is achieved by simply replacing η in Eq. (2) with our calculated electron width. We found that the electron width is large enough to explain a major part of the large broadening effect at the interband transition edge. This means that other broadening effects, e.g., effects due to the c-axis dispersion, are probably not very important.

In the next section we present the theory of the lifetime calculation for electrons in the conduction band. The numerical results are demonstrated and discussed in Sec. III. The calculated inverse lifetime is then used in Sec. IV for the calculation of the interband transition spectrum, i.e., $\mathrm{Im}\epsilon_{v\text{-}c}(\omega)$. Finally, Sec. V contains the concluding remarks.

II. THEORY OF THE LIFETIME CALCULATION

In this section we follow closely the method of Giuliani and Quinn[6] in calculating the lifetime of an electron in the conduction band. But unlike the 2D electron gas of Giuliani and Quinn, a GIC is composed of a periodic array of graphite layers and each layer contains both a conduction band and a partially filled valence band. Because of the complicated band structure, there exist various decay channels for a conduction electron. Note that there are two valleys in the system (U and U'). As a result, electrons can decay through both intravalley and intervalley processes. Since the two kinds of processes provide equivalent densities of states for decaying, both should be kept in the lifetime calculation. For the reason that the U and U' points are well separated, we can study the intravalley processes first and include the intervalley processes afterwards.

Allowed decay processes are plotted in Fig. 2. Dot-shaded regions represent the electronic excitation spectrum—including a plasmon band,[7] and line-shaded regions are possible decay channels from phase-space considerations—the region a from the intraband transitions and the region b from interband transitions. In order to keep the energy and the momentum conserved, only the deexcitations which are inside the overlapped regions (between the two shading patterns) are actually allowed decay processes. One special feature of the system is that only interband deexcitations can decay into plasmons. Since plasmon modes provide an efficient deexcitation channel for the electrons, we can expect that interband

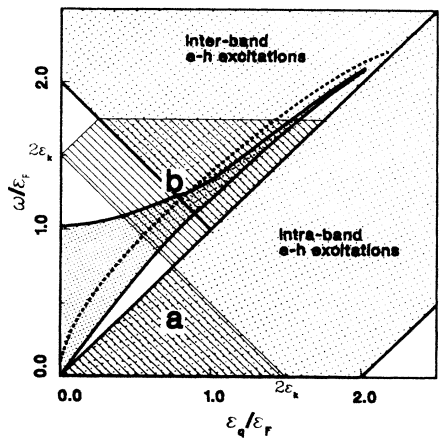

FIG. 2. The excitation spectrum of the system is shown by the dotted regions, which include both the electron-hole excitations (as indicated) and the plasmons (shown by the densely dotted band). Also shown is the 2D plasmon curve (the dashed curve) for a single graphite layer. Line-shaded regions demonstrate possible deexcitations for a conduction electron with the energy $\varepsilon_k = 0.75\varepsilon_F$. The regions denoted by a and b correspond, respectively, to the intraband process and the interband process. Only the deexcitations in the regions that overlap with the electron-excitation spectrum are actually allowed. It is obvious from this figure that only through interband processes can an electron decay into a plasmon.

transitions contribute the most important part to the lifetime calculation.

Detailed calculations of the electron lifetime are given in the following subsections.

A. The intraband process

Following the practice of the Appendix, we denote graphite layers by an index l, which corresponds to the layer position at $z=lI_c$ (I_c is the distance between graphite layers). In our superlattice model, the number of the graphite layers is infinite, i.e., $-\infty<l<+\infty$. In this case, all surface effects are ignored; thus we can consider that the decaying conduction electron ε_k^c is on the layer $l_0=0$. To calculate the lifetime due to intraband deexcitations, we use the golden rule,[6,8] and obtain ($\hbar=1$)

$$\left[\frac{1}{\tau_k}\right]_a=2\pi\sum_{\mathbf{p},\mathbf{q}}\sum_l n^v_{p,l}(1-n^v_{|\mathbf{p}-\mathbf{q}|,l})(1-n^c_{|\mathbf{k}+\mathbf{q}|,l_0})\,|V_l(\mathbf{p},\mathbf{k},\mathbf{q})|^2\delta(\varepsilon^v_{|\mathbf{p}-\mathbf{q}|,l}+\varepsilon^c_{|\mathbf{k}+\mathbf{q}|,l_0}-\varepsilon^v_{p,l}-\varepsilon^c_{k,l_0})\,. \tag{4}$$

In this expression, $n^{v(c)}_{p,l}$ is the occupation function for the p state in the valence (conduction) band of the layer l; the energy of the state is denoted by $\varepsilon^{v(c)}_{p,l}$. Since all layers are identical to each other, we only need to keep the layer index in $V_l(\mathbf{p},\mathbf{k},\mathbf{q})$, the matrix element of the Coulomb interaction. As will be shown below, the major task in evaluating Eq. (4) is that the Coulomb interaction is l dependent and, meanwhile, this interaction must be properly screened.

We find that the calculation of the matrix element can be done easily in the h_z space, which is defined according to the Fourier transformation expressed by Eq. (A3). In terms of Parseval's theorem, the summation over l in Eq. (4) can be carried out in the h_z space. Then, by using Eq. (A4), we get

$$\sum_l|V_l(\mathbf{p},\mathbf{k},\mathbf{q})|^2=\frac{I_c}{2\pi}\int_{-\pi/I_c}^{\pi/I_c}dh_z\left|\frac{v^{\rm ex}_{h_z}(\mathbf{p},\mathbf{k},\mathbf{q})}{\epsilon(q,h_z,\omega)}\right|^2_{\omega=\varepsilon^c_k-\varepsilon^c_{|\mathbf{k}+\mathbf{q}|}} \tag{5}$$

The dielectric function $\epsilon(q,h_z,\omega)$ is known from Eq. (A5), and $v^{\rm ex}_{h_z}(\mathbf{p},\mathbf{k},\mathbf{q})$ is the unscreened matrix element which we can analytically evaluate in terms of the Bloch states obtained from the 2D calculation of Blinowski *et al.*[2] The matrix element of Coulomb interaction has been evaluated in Ref. 7 and has the result

$$v^{\rm ex}_l(\mathbf{p},\mathbf{k},\mathbf{q})=\tfrac{1}{2}v_qI^2(q)\left[1+\frac{k+q\cos\phi}{|\mathbf{k}+\mathbf{q}|}\right]e^{-q|z|}\Big|_{z=lI_c}, \tag{6}$$

where $v_q=2\pi e^2/q$, ϕ is the angle between $\mathbf{k}$ and $\mathbf{q}$, and $I^2(q)$ is a factor very close to one for intravalley processes [e.g., $I^2(k_F)=0.993$ if $\varepsilon_F=1$ eV; see Ref. 7 for details]. By performing a Fourier transformation for $v^{\rm ex}_l(\mathbf{p},\mathbf{k},\mathbf{q})$ and using the results of Eqs. (5) and (6), we have

$$\left[\frac{1}{\tau_k}\right]_a=\sum_{\mathbf{q}}\int d\omega\,v_qI^2(q)\left[1+\frac{k+q\cos\phi}{|\mathbf{k}+\mathbf{q}|}\right](1-n^c_{|\mathbf{k}+\mathbf{q}|})\delta(\omega-\varepsilon^c_k+\varepsilon^c_{|\mathbf{k}+\mathbf{q}|})\frac{I_c}{2\pi}\int_{-\pi/I_c}^{\pi/I_c}dh_z\,S(q,h_z)\,{\rm Im}\left[\frac{-1}{\epsilon(q,h_z,\omega)}\right], \tag{7}$$

where $S(q,h_z)$, $\epsilon(q,h_z,\omega)$, and $\chi^a(q,\omega)$ are defined in the Appendix. The integration over h_z has been exactly evaluated and the dimensionless result is denoted by ${\rm Im}[-1/\epsilon^s(q,\omega)]$ and given by Eqs. (A9) and (A10). After carrying out the integration over the angle of $\mathbf{q}$, we finally obtain

$$\left[\frac{1}{\tau_k}\right]_a=\frac{e^2}{\pi v_F}\int_0^{\varepsilon_k}d\omega\int_\omega^{2\varepsilon_k-\omega}d\varepsilon_q\frac{I^2(q)}{\varepsilon_k}\left[\frac{(2\varepsilon_k-\omega)^2-\varepsilon_q^2}{\varepsilon_q^2-\omega^2}\right]^{1/2}{\rm Im}\left[\frac{-1}{\epsilon^s(q,\omega)}\right]. \tag{8}$$

Equation (8) needs to be numerically evaluated and this can be done easily because all terms in the integrand have been analytically derived.

B. The interband process

As we mentioned earlier in this section, a conduction electron, through interband deexcitation, can decay either into an electron-hole pair or into a plasmon. Therefore, it is convenient to express the inverse lifetime due to interband processes as the sum of two terms,

$$\left[\frac{1}{\tau_k}\right]_{\rm interband}=\left[\frac{1}{\tau_k}\right]_b+\left[\frac{1}{\tau_k}\right]_{\rm pl},$$

with the obvious subscripts indicating the two decay interband channels. The calculation here is very similar to that of the interband process, and hence we only present the result:

$$\left[\frac{1}{\tau_k}\right]_b+\left[\frac{1}{\tau_k}\right]_{\rm pl}=\frac{e^2}{\pi v_F}\int_{\varepsilon_k}^{\varepsilon_k+\varepsilon_F}d\omega\int_{|2\varepsilon_k-\omega|}^{\omega}d\varepsilon_q\frac{I^2(q)}{\varepsilon_k}\left[\frac{\varepsilon_q^2-(\omega-2\varepsilon_k)^2}{\omega^2-\varepsilon_q^2}\right]^{1/2}\mathrm{Im}\left[\frac{-1}{\epsilon^s(q,\omega)}\right]. \tag{9}$$

The integration limits are determined by the requirement that the final state $(\mathbf{k}+\mathbf{q})$ stays above the Fermi level. The line-shaded region b in Fig. 2 represents the allowed deexcitations confined by these integration limits for the case $\varepsilon_k=0.75\varepsilon_F$. It is clear from this figure that $(1/\tau_k)_b$ and $(1/\tau_k)_{\rm pl}$ correspond, respectively, to the regions where $\omega>2\varepsilon_F-\varepsilon_q$ and $\omega<2\varepsilon_F-\varepsilon_q$.

Regarding plasmons, we have the following three remarks: First, plasmon resonances in the region $\omega>2\varepsilon_F-\varepsilon_q$, despite the fact that they are damped due to interband excitations, constitute a major structure of $\mathrm{Im}[-1/\epsilon^s(q,\omega)]$ and therefore provide important contributions to $(1/\tau_k)_b$; second, the plasmon decay channel is closed, i.e., $(1/\tau_k)_{\rm pl}=0$, if the initial state has an energy ε_k^c greater than ε_F (this can be easily seen from Fig. 3); and third, because plasmons provide very efficient decay channels, the interband processes are the most important ones for the deexcitation of an conduction electron in GIC's. These remarks will be numerically examined in the next section, after we study the intervalley processes.

C. The intervalley process

The intervalley processes are deexcitations in which a conduction electron is scattered from a state close to the U point to a state near the U' point. Because the band structure near one corner is identical to that near another, we find that the lifetime calculations are similar to those of intravalley transitions. It is clear that, for an intravalley transition from $\mathbf{k}$ to $\mathbf{k}+\mathbf{q}$, there is a corresponding intervalley transition from $\mathbf{k}$ to $\mathbf{k}+\Delta\mathbf{U}+\mathbf{q}$, where the vector $\Delta\mathbf{U}$ links U and U'. With the large momentum transfer $(\Delta\mathbf{U}+\mathbf{q})$, the anisotropic nature of the system is now involved, i.e., the lifetime is $\mathbf{k}$ dependent. Nevertheless, the anisotropic effects are small and we can eliminate them by applying a proper approximation.

We now proceed to formulate $(1/\tau_k)_{a'}$ and $(1/\tau_k)_{b'}$—the inverse of the electron lifetime due to intervalley intraband transitions and intervalley interband transitions, respectively. Let us consider the intraband transitions first. It is found that we can use Eq. (4) to calculate $(1/\tau_k)_{a'}$ with only the modification of using an appropriate matrix element $V_l(\mathbf{p},\mathbf{k},\Delta\mathbf{U}+\mathbf{q})$ in the place of $V_l(\mathbf{p},\mathbf{k},\mathbf{q})$ therein. The evaluation of this matrix element follows closely that shown in Eqs. (5)—(7), but before the calculation one requires a dielectric function for large momentum transfer, so that the Coulomb interaction can be properly screened. For this purpose, we can approximate $|\Delta\mathbf{U}+\mathbf{q}|$ by $|\Delta\mathbf{U}|$, since $|\Delta U|$ $(4\pi/3\sqrt{3}b$, $b=1.42$ Å) is much larger than the average of $q\sim k_F$ (e.g., for $\varepsilon_F=1$ eV, a typical value for GIC's, $|\Delta\mathbf{U}|/k_F=8.7$). With this approximation, we can immediately write

$$\varepsilon(|\Delta\mathbf{U}+\mathbf{q}|,h_z,\omega)\approx\epsilon_0-v_{|\Delta\mathbf{U}|}S(|\Delta\mathbf{U}|,h_z)\frac{I^2(|\Delta\mathbf{U}|)}{2I^2(q)}[\chi^a(q,\omega)+\chi^b(q,\omega)], \tag{10}$$

where $v_{|\Delta U|}=2\pi e^2/|\Delta\mathbf{U}|$, $I^2(|\Delta\mathbf{U}|)=0.63$, and $\chi^{a,b}(q,\omega)$ are, as defined in Eq. (A2'), the response functions for the momentum transfer $\mathbf{q}$—not for $\Delta\mathbf{U}+\mathbf{q}$. Equation (10) follows directly from Eq. (A5) and the relation that

$$\chi^{a,b}(|\Delta\mathbf{U}+\mathbf{q}|,\omega)\approx\frac{1}{2}\frac{I^2(|\Delta\mathbf{U}|)}{I^2(q)}\chi^{a,b}(q,\omega). \tag{11}$$

The factor of $\frac{1}{2}$ on the right-hand side of (11) is due to the fact that the number of possible excitations at the momentum transfer $(\Delta\mathbf{U}+\mathbf{q})$ is exactly one-half that at the momentum transfer $\mathbf{q}$. Now that the dielectric function is determined, the rest of the calculation parallels that of Eqs. (4)—(8) and yields the result

$$\left[\frac{1}{\tau_k}\right]_{a'}=\frac{e^2}{\pi v_F}\int_0^{\varepsilon_F}d\omega\int_{\omega}^{2\varepsilon_F-\omega}d\varepsilon_q\left[\frac{q}{|\Delta\mathbf{U}|}\right]\frac{I^2(|\Delta\mathbf{U}|)}{\varepsilon_k}\left[\frac{(2\varepsilon_k-\omega)^2-\varepsilon_q^2}{\varepsilon_q^2-\omega^2}\right]^{1/2}\mathrm{Im}\left[\frac{-1}{\epsilon^s(|\mathbf{q}+\Delta\mathbf{U}|,\omega)}\right]. \tag{12}$$

Similar arguments can be applied to intervalley interband transitions. By doing so, we readily obtain

$$\left[\frac{1}{\tau_k}\right]_{b'}=\frac{e^2}{\pi v_F}\int_{\varepsilon_k}^{\varepsilon_k+\varepsilon_F}d\omega\int_{|2\varepsilon_k-\omega|}^{\omega}d\varepsilon_q\left[\frac{q}{|\Delta\mathbf{U}|}\right]\frac{I^2(|\Delta\mathbf{U}|)}{\varepsilon_k}\left[\frac{\varepsilon_q^2-(\omega-2\varepsilon_k)^2}{\omega^2-\varepsilon_q^2}\right]^{1/2}\mathrm{Im}\left[\frac{-1}{\epsilon^s(|\mathbf{q}+\Delta\mathbf{U}|,\omega)}\right]. \tag{13}$$

Equations (12) and (13) are not suitable for numerical calculations.

III. THE CALCULATED LIFETIME

The total of the inverse lifetime is the sum of Eqs. (8), (9), (12), and (13). This sum is related to the imaginary part of the self-energy of a conduction electron, $\Sigma_2(k)$, by the relation[6,8]

$$\Sigma_2(k)=\frac{1}{2}\left[\left[\frac{1}{\tau_k}\right]_a+\left[\frac{1}{\tau_k}\right]_{a'}+\left[\frac{1}{\tau_k}\right]_b+\left[\frac{1}{\tau_k}\right]_{b'}+\left[\frac{1}{\tau_k}\right]_{\rm pl}\right]. \tag{14}$$

Since this is the only broadening effect that we intend to investigate here, we can set

$$\Gamma_k = \Sigma_2(k) , \tag{15}$$

where Γ_k denotes the width associated with the interband transition from ε_k^v to ε_k^c.

Before we can calculate Γ_k, we need to determine ϵ_0 for GIC's. From the measurement of Taft and Philipp,[9] it can be inferred that ϵ_0 is 2.4 for pure graphite. We assume that high-energy excitations are not appreciably affected by intercalation, and thus will use $\epsilon_0 = 2.4$ in the following calculation for intercalated graphite systems.

After ϵ_0 is determined, the calculation of Γ_k is numerically straightforward. Figure 3 demonstrates the results from such calculations for a system with $\varepsilon_F = 1$ eV. In addition to the width Γ_k (the thick solid curve), the accumulated contributions from different deexcitation channels are also shown (the thin solid curves). The curve a denotes $(1/\tau_k)_a$, and other thin curves are denoted in a similar fashion. The most outstanding feature found in this calculation is the structure due to plasmons—the "hump" at $\varepsilon_k \sim 0.5\varepsilon_F$. As we have explained earlier, this structure is the result of interband transitions, in which a conduction electron can either decay into an undamped plasmon, i.e., $(1/\tau_k)_{\rm pl}$, or into a damped plasmon; the contribution of the latter is contained in $(1/\tau_k)_b$. Due to the special band structure of the system, the plasmon channel is most active when $\varepsilon_k \approx 0.5\varepsilon_F$, as can be seen easily from Fig. 2. Also according to Fig. 2, we find, if $\varepsilon_k > \varepsilon_F$, not only that undamped plasmon modes are no longer available for decaying [i.e., $(1/\tau_k)_{\rm pl} = 0$], but also that damped plasmons are less and less involved in the decay process as ε_k becomes larger. This observations explains why Γ_k reaches a maximum at $\varepsilon_k \approx 0.5\varepsilon_F$ and then decreases at larger ε_k. This feature can be understood only when dynamic screening is included, since, as ε_k increases, one would actually expect Γ_k to increase for the reason that there would be more vacant states available for decaying. It should be noticed that the increased number of vacant states as ε_k increases are accessible only through intraband processes, in which the plasmon modes are not involved. Therefore, only the part due to intraband deexcitations (the curve a) increases concurrently with ε_k. At energies higher than $1.5\varepsilon_F$, intraband transitions might become the dominating part (depending on ε_F); then, Γ_k would increase with ε_k. From Fig. 3 it is clear that intervalley processes are not important compared with their intravalley counterparts—they are about an order of magnitude smaller.

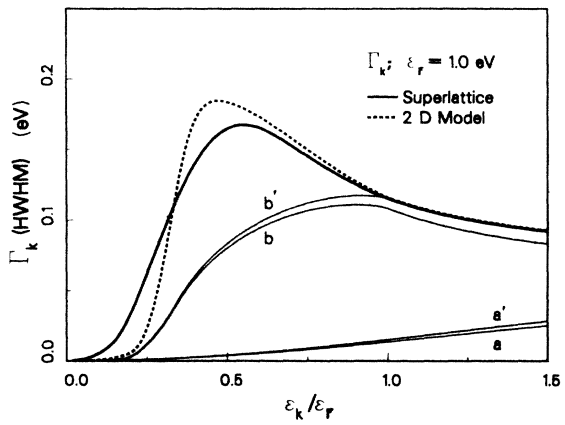

FIG. 3. We show in this figure the calculated width (the thick solid curve) of a conduction electron, as a function of its energy ε_k. In this calculation, we use $\varepsilon_F = 1$ eV, a typical Fermi energy for a stage-1 compound. Accumulated contributions from various decay channels are also shown, by the thin solid curves which are denoted according to the subscripts of Eq. (14). Between the curve b' and the total width is the part due to the plasmon channel. Because of the plasmon mode, the width has a maximum at $\varepsilon_k = 0.5\varepsilon_F$. The dashed curve is the width calculated for a single graphite layer. Note that there is no qualitative difference between the two calculations—meaning the 2D model is a good approximation for the 3D system of GIC's.

The dashed curve in Fig. 3 is calculated for a system with only one graphite layer. This calculation is performed according to relations similar to Eqs. (8) (9), (12), and (13), but by substituting $\mathrm{Im}[-1/\epsilon^s(q,\omega)]$ therein with $\mathrm{Im}[-1/\epsilon^{2D}(q,\omega)]$. $\epsilon^{2D}(q,\omega)$ is given by Eq. (A2). This 2D calculation is interesting because, for a layer system like a GIC, we would like to know how important the presence of other layers, or the 3D behavior, is. In the weak-coupling limit ($qI_c \gg 1$), one can easily show that

$$\mathrm{Im}[-1/\epsilon^s(q,\omega)] = \mathrm{Im}[-1/\epsilon^{2D}(q,\omega)] ,$$

i.e., 3D characteristics disappear. In the strong-coupling region ($qI_c \ll 1$), the plasmon spectra of the two systems are very different (see Fig. 2); thus, different results are expected. Our calculation shows that the 2D result is only quantitatively, not qualitatively, different from the 3D result. In fact, only the detailed structure at $\varepsilon_k \sim 0.5\varepsilon_F$, i.e., the part that depends on plasmons, differs. For $\varepsilon_k > \varepsilon_F$, where the effects due to plasmons are diminishing, the 2D result is practically undistinguishable from its 3D counterpart. We notice that a typical momentum transfer in electron-hole excitations is $\sim k_F$ and $k_F I_c = 1.8$ if ε_F is 1 eV. This means that electron-hole excitations are mostly in the weak-coupling regime, or, put differently, that they are dominated by the 2D behavior. Since the typical Fermi energy of a low-stage GIC is about 1 eV, we can conclude, according to our calculation, that, except for plasmons, electronic excitations of a low-stage GIC can be well approximated by using a 2D model.

The present theory only depends on the charge density in graphite layers. Therefore, it can be applied easily to systems with different Fermi energies. Figure 4 demonstrates results from such calculations with ε_F between 0.5 and 1.5 eV. We find the similar structure in all curves—a "hump" at $\varepsilon_k = 0.5\varepsilon_F$, obviously due to plasmon excitations. The magnitude of Γ_k is larger for systems with higher Fermi energies, as may have been expected based on a phase-space consideration.

As has been discussed, Γ_k is determined principally by the in-plane properties of a graphite layer. The presence of other graphite layers only results in minor modifications; these modifications are mostly due to plasmons and are in the region $\varepsilon_k < \varepsilon_F$. For optical transitions in GIC's, only states with $\varepsilon_k > \varepsilon_F$ are involved, and hence the associated lifetime effect is mostly determined by the in-plane

properties and not appreciably affected by the intercalation. Based on this finding, we thus expect that our theory should not be restricted to the application of stage-one GIC's, but should describe other low-stage systems as well, at least qualitatively. In the next section we will apply the present calculation to investigate the edge structure of optically induced interband transitions—for stage-1 as well as for stage-2 GIC's.

IV. THE EDGE STRUCTURE

We have calculated the width Γ_k associated with the interband transitions in GIC's. Replacing this Γ_k with η in Eq. (2), we can evaluate the spectrum of interband transitions according to the relation

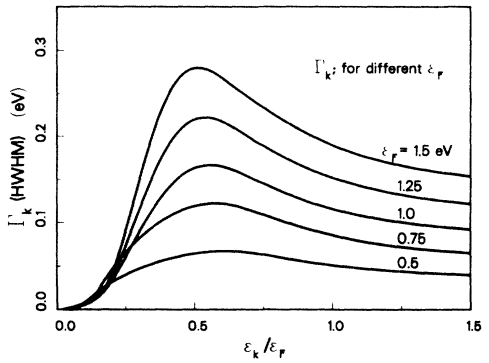

FIG. 4. A calculation similar to that of Fig. 3 is repeated here for different Fermi energies. Notice that the maximum at $\varepsilon_k=0.5\varepsilon_F$, which is a feature due to plasmons, is found in all curves.

$$\mathrm{Im}\epsilon_{v\text{-}c}(\omega)=\frac{4e^2}{I_c}\int d\omega_k \frac{\omega_k\Gamma_k}{[(\omega^2-\omega_k^2)^2+\Gamma_k^2(\Gamma_k^2+2\omega^2+\omega_k^2)]}\frac{1}{[1+e^{(2\varepsilon_F-\omega_k)/2k_BT}]}\quad(\omega_k=2\varepsilon_k)\,. \tag{16}$$

Note that the temperature-broadening factor, which has been kept in the formalism, is not too small an effect, since the thermal broadening is doubled (to $2k_BT$) in the interband transitions. For example, at $T=300$ K, $2k_BT$ is about 0.05 eV, or nearly one-half the size of Γ_k, for $k=k_F$ and $\varepsilon_F=1$ eV (see Fig. 3). In what follows, we will calculate the spectra for the stage-1 ($n=1$) and stage-2 ($n=2$) GIC's, and compare them with the measurement by Hoffman *et al.*[1]

Our calculated results are given by the solid curves, and the measured ones by dotted lines in Fig. 5. In this calculation, we have used the Fermi energies that would produce the correct edge positions, i.e., ε_F is 0.98 eV if $n=1$ and 0.89 eV if $n=2$.[1] One should notice that these Fermi energies differ from those obtained by using a different method[1] (see below). From Fig. 5 it is obvious that the broadening is not fully explained by our calculation in the $n=1$ case, although the edge structure is very well reproduced in the $n=2$ case. The comparison can be made more specific if we convert all the broadening factors into an effective temperature, and compare it with the effective temperature that is needed in order to describe the measured edge structure. The latter has already been obtained by Hoffman *et al.*[1] For the $n=1$ system, we find that $\Gamma_k/2k_B+T=950$ K at $k=k_F$, while the measured effective temperature is 1400 K, i.e., the present calculation has only explained two-thirds of the broadening found experimentally. For the $n=2$ system, we find that $\Gamma_k/2k_B+T\approx 850$ K, which is slightly larger than the estimated effective temperature of 750 K. In order to make direct comparison with the measurement, the calculated results have been multiplied by constant factors (e.g., for $n=1$, the factor is 1.8). Other calculations[1,5] based on Eq. (3), or its equivalent, also find similar disagreement regarding the magnitude of the interband transitions, and there is no explanation for it so far.

Although our calculations have been able to explain a large part of the broadening found at the edge of interband transitions, the existing discrepancy between the calculation and the measurement needs some explanation. Let us confine ourselves to the $n=1$ system in this regard, because this is the system where a large discrepancy is found, and also because this is the system our theory is built for, although the theory can be applied to other low-stage GIC's for qualitative investigations. Firstly, about the edge position, we note that the prediction that the edge should be at $2\varepsilon_F$ (Fig. 1) is based on a picture for a noninteractive system, in which the electron-electron in-

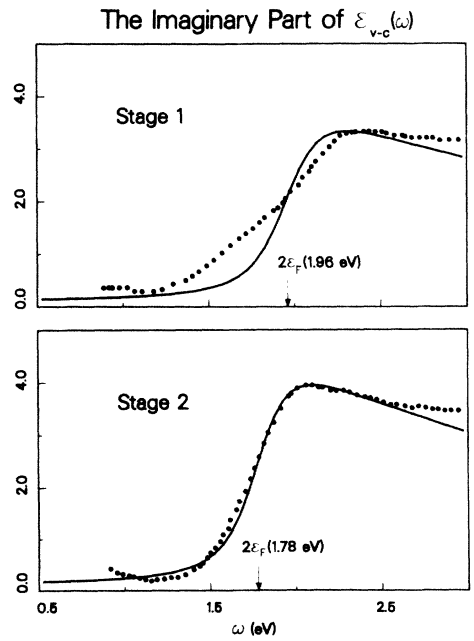

FIG. 5. The calculated spectra of optically induced interband transitions (the solid curves) and the measured spectra (the dotted line) are shown in this figure. We find a better agreement for the stage-2 case than for the stage-1 case. See the main text for ways to improve our present calculation.

teraction is excluded. In fact, an optical transition is a two-body problem since an electron and a hole are created in the transition, and the two can interact via the Coulomb force (the exciton effect). It has been shown[8,10] that this attractive force tends to lower the edge position of an interband transition. In the experiment with GIC's, Hoffman *et al.* used a relation between the Fermi energy and the plasmon energy, which is directly measurable, and found that the Fermi energy is 1.28 eV. This value is considerably higher than the one we used according to the edge position (0.98 eV). If we use this alternatively determined ε_F to calculate Γ_k, we find that $\Gamma_k/2k_B+T=1250$ K (see Fig. 4), which is now much closer to the expected value of 1400 K. Second, besides the scattering mechanism which we have considered in our calculation, there are other scattering channels which also can contribute to the edge-broadening effect. Some of those uncounted channels, like the initial-state broadening and the phonon scattering, are probably not important for the edge spectra, as we have explained in the Introduction. However, the scattering of electrons by intercalants, which we did not include in the calculation, might be important, since the intercalants now carry net charges and the Coulomb potential is strong and long ranged. Inclusion of this effect could help to better explain the edge structure.

It should be pointed out here that the exciton effect and the lifetime effect are not unrelated effects in the optical transition. The former causes a singularity at the edge, while the latter smooths, or even suppresses, this anomaly at threshold.[10] It can also be inferred from Ref. 10 that the larger the electronic width the stronger the downshift of the edge from the position which would be expected from using a single-particle picture. Experimental evidence shows no anomaly at the edge (see Fig. 5), suggesting that the electronic width is large enough to suppress it. Recent measurement[11] also shows that there is a consistent downshift ($\sim$0.5 eV) of the optical transition edge in various $n=1,2$ GIC's, indicating that the exciton effect is important. Therefore, it is clear that, in order to interpret the threshold structure, we need to evaluate lifetime accurately and study its effect concurrently with the exciton effect.

From our calculations shown by Fig. 5 and from our discussion given above, it can be concluded that the edge-broadening effect found in the interband spectra is principally due to the scattering of the final-state electron in the conduction band. To improve our theory, we need to closely examine the exciton effect in GIC. This is possible now because a reliable dielectric function for the system is available,[7] which is needed in describing the screened Coulomb interaction between the electron and the hole. Also of importance is the inclusion of other scattering mechanisms, especially that due to intercalants, into the scheme. Modification of our theory in these directions will be studied in a planned future work.

V. CONCLUSION

In this paper, we have presented a detailed calculation of the lifetime of an electron, which is in the conduction band of a stage-1, acceptor-type GIC. These calculated results were than applied to explain the edge structure of optically induced interband transitions. The edge structure of both the stage-1 and the stage-2 compounds have been examined. In both cases, the lifetime broadening of the final-state electron was found to be the main reason for the edge-broadening effect.

Two notable features from the lifetime calculation are, first, that because of the efficient decay channel due to plasmons, the inverse lifetime reaches a maximum at $\varepsilon_k\sim 0.5\varepsilon_F$, and second, that the lifetime can be quite well approximated by a 2D calculation. This latter finding is somewhat surprising since the plasmons of the system show explicit 3D characteristics.[7] One can conclude accordingly that, for an intercalated graphite system, the presence of neighboring graphite layers is not important, unless one is looking at plasmons specifically.

For the broadening effect at the edge of interband transitions, we can improve our treatment by taking into account the exciton effect and by including other scattering mechanisms. Both of these suggested modifications should increase the inverse lifetime of the final-state electron, and would thus help better explain the edge structure.

One last point we would like to address concerns the generalization of our theory. One example in this regard has been demonstrated in the calculation of the spectrum for stage-2 GIC's. There, we have found close agreement with the measured result. Another category of the generalization of our theory is to extend it to donor-type GIC's. In practice, we do not even need to change the formalisms that we have developed for acceptor-type compounds [e.g., the dielectric function, the electron width, and $\mathrm{Im}\epsilon_{v\text{-}c}(\omega)$] in order to describe the donor-type compounds. The reason for this is that, by replacing the electron states in one system with the hole states of the other, our theory remains unchanged. Accordingly, our theory predicts that the spectrum of the interband transitions from a donor-type compound should be identical to the one from an acceptor-type compound, if the two compounds have the same stage of intercalation and the same Fermi energy. Comparing these two spectra experimentally, therefore, should reveal valuable information on the basic assumption we have made, which is also the assumption that is generally made;[1,2] that is, except for the position of the Fermi level, it is assumed that intercalants do not affect the electronic structure and its properties. This kind of experiment should be a crucial test of our theory.

ACKNOWLEDGMENTS

The author thanks Professor G. D. Mahan for suggesting this problem and for helpful discussions. He also wishes to thank B. Sernelius for stimulating discussions, and D. Meltzer for a critical reading of the manuscript. This research was sponsored jointly by the National Science Foundation through Grant No. DMR-85-01101, and by the Division of Materials Sciences, U.S. Department of Energy, under Contract No. DE-AC05-84OR21400 with Martin Marietta Energy Systems, Inc., through the

University of Tennessee—Oak Ridge National Laboratory Distinguished Scientist Program.

APPENDIX

We summarize in this Appendix the results from Ref. 7, where we have calculated the dielectric function of GIC's. We will first describe the dielectric function of a single graphite layer (the 2D model) in subsection 1, and then the dielectric function of three-dimensional GIC's (the superlattice model) in subsection 2. The calculation of the loss function of the superlattice model, $\mathrm{Im}[-1/\epsilon^s(q,\omega)]$ (to be defined below), is contained in subsection 3.

1. A single graphite layer

With the presence of highly mobile charge carriers in the system, an external potential $v^{\mathrm{ex}}(q,\omega)$ is accompanied by an induced field. As a result, electrons in the graphite layer feel a screened potential

$$v^{\mathrm{sc}}(q,\omega)=\frac{v^{\mathrm{ex}}(q,\omega)}{\epsilon^{\mathrm{2D}}(q,\omega)} . \tag{A1}$$

This expression defines the dielectric function $\epsilon^{\mathrm{2D}}(q,\omega)$, where the superscripts 2D indicates that there is only one graphite layer in the system. Because there are both intraband and interband transitions, the dielectric function can be expressed by

$$\epsilon^{\mathrm{2D}}(q,\omega)=\epsilon_0-v_q\chi^a(q,\omega)-v_q\chi^b(q,\omega) , \tag{A2}$$

where ϵ_0 is the background screening constant, the second and the third terms, respectively, describe the intraband and the interband transitions, and $v_q=2\pi e^2/q$ is the 2D Coulomb potential. The response function $\chi^a(q,\omega)$ is defined by

$$\chi^a(q,\omega)=4\sum_{\mathbf{k}}|\langle \mathbf{k};v\,|\,e^{-i\mathbf{q}\cdot\mathbf{r}}\,|\,\mathbf{k}+\mathbf{q};v\rangle|^2 \times\frac{n^v_{\mathbf{k}+\mathbf{q}}-n^v_{\mathbf{k}}}{\varepsilon^v_{\mathbf{k}+\mathbf{q}}-\varepsilon^v_{\mathbf{k}}-\omega+i\eta} , \tag{A2'}$$

with obvious notation, and the factor of 4 accounts for the spin and the two valleys; $\chi^b(q,\omega)$ is defined similarly. These two response functions have been analytically evaluated, and are given in Appendix A of Ref. 7. Two points worthy of notice are, first, that our calculation is essentially exact according to the band structure from the 2D model, and second, that, basically, $\epsilon^{\mathrm{2D}}(q,\omega)$ only depends on the density of the free charges in the system (or equivalently, depends on ε_F)—i.e., no adjustable parameter is needed in the formalism.

2. The superlattice model of GIC's

This model has been described in the Introduction. According to the model, there are infinitely many graphite layers in the system, and each is denoted by a layer index l $(-\infty<l<+\infty)$. With this structure, the external potential $v_l^{\mathrm{ex}}(q,\omega)$, and the screened potential $v_l^{\mathrm{sc}}(q,\omega)$ are, as indicated by their notations, layer dependent. We define the Fourier transform of these potentials as follows,

$$\sum_l v_l^{\mathrm{ex}}(q,\omega)e^{ih_zlI_c}=v^{\mathrm{ex}}(q,h_z,\omega)$$

and

$$\sum_l v_l^{\mathrm{sc}}(q,\omega)e^{ih_zlI_c}=v^{\mathrm{sc}}(q,h_z,\omega) , \tag{A3}$$

where h_z is confined to the first Brillouin zone, i.e., $|h_z|<\pi/I_c$. The dielectric function of the superlattice is defined, similarly to Eq. (A2), by the relation

$$v^{\mathrm{sc}}(q,h_z,\omega)=\frac{v^{\mathrm{ex}}(q,h_z,\omega)}{\epsilon(q,h_z,\omega)} , \tag{A4}$$

and can be expressed compactly:

$$\epsilon(q,h_z,\omega)=\epsilon_0-v_qS(q,h_z)[\chi^a(q,\omega)+\chi^b(q,\omega)] . \tag{A5}$$

Compared with $\epsilon^{\mathrm{2D}}(q,\omega)$ of Eq. (A2), $\epsilon(q,h_z,\omega)$ contains an extra structure factor $S(q,h_z)$ that describes the layer structure:

$$S(q,h_z)=\sum_l e^{-q|l|I_c+ih_zlI_c}=\frac{\sinh(qI_c)}{\cosh(qI_c)-\cos(h_zI_c)} . \tag{A6}$$

The effect of this structure factor is to modify the Coulomb interaction. In the small-q limit, we find

$$\lim_{q\to0}\lim_{h_z\to0}[v_qS(q,h_z)]=\frac{4\pi e^2}{q^2I_c} , \tag{A7}$$

which means the interaction is three dimensional.

3. The calculation of $\mathrm{Im}[-1/\epsilon^s(q,\omega)]$

The energy-loss function of GIC's is defined by

$$\mathrm{Im}\left[\frac{-1}{\epsilon^s(q,\omega)}\right]=\frac{I_c}{2\pi}\int_{-\pi/I_c}^{\pi/I_c}dh_z\,S(q,h_z) \times\mathrm{Im}\left[\frac{-1}{\epsilon(q,h_z,\omega)}\right] , \tag{A8}$$

which has two separate contributions from electron-hole excitations and from plasmons. The part from e-h excitations [where $\epsilon_2(q,h_z,\omega)\neq0$] is analytically evaluated:

$$\mathrm{Im}\left[\frac{-1}{\epsilon^s(q,\omega)}\right]=\frac{2\pi A}{\nu|s^2-1|} \times\left[\frac{|s^2-1|-\mu^2+\nu^2+1}{2}\right]^{1/2} , \tag{A9}$$

where

$$|s^2-1|=[(\gamma-1)^2+4\nu^2]^{1/2} .$$

The variables in this expression have the values

$$A=\frac{v_q\chi_2(q,\omega)\sinh^2(qI_c)}{2\pi\epsilon_0^2}\ ,$$

$$\beta=-2\mu=-2\left[\cosh(qI_c)+\frac{v_q\chi_1(q,\omega)}{\epsilon_0}\sinh(qI_c)\right]\ , \tag{A10}$$

$$\gamma=\mu^2+\nu^2\ ,$$

$$\nu=\frac{v_q\chi_2(q,\omega)}{\epsilon_0}\sinh(qI_c)\ .$$

For the plasmon part [where $\epsilon_2(q,h_z,\omega)=0$], we found in Ref. 7 that

$$\mathrm{Im}\left[\frac{-1}{\epsilon^s(q,\omega)}\right]=\frac{\pi\sinh(qI_c)}{\epsilon_0'\sin(h_zI_c)}\ , \tag{A11}$$

where h_z satisfies the relation $\omega=\omega_p(q,h_z)$. The plasmon energy $\omega_p(q,h_z)$ is determined by the zeros of $\epsilon(q,h_z,\omega)$. The background screening factor ϵ_0' now includes the contribution due to the interband transitions and hence varies as a function of q, h_z, and ω (see Ref. 7).

[1]D. M. Hoffman, R. E. Heinz, G. L. Doll, and P. C. Eklund, Phys. Rev. B. **32**, 1278 (1985).
[2]J. Blinowski, Nguyen Hy Hau, C. Rigaux, J. P. Vieren, R. le Toullee, G. Furdin, A. Herold, and J. Melin, J. Phys. (Paris) **41**, 47 (1980).
[3]J. Blinowski and C. Rigaux, J. Phys. (Paris) **41**, 667 (1980).
[4]T. Ohno, N. Shima, and H. Kamimura, Solid State Commun. **44**, 761 (1982).
[5]D. F. Hoffman, P. C. Eklund, R. E. Heinz, P. Hawrylak, and K. R. Subbaswamy, Phys. Rev. B **31**, 3973 (1985).
[6]G. F. Giuliani and J. Quinn, Phys. Rev. B **26**, 4421 (1982).
[7]K. W.-K. Shung, Phys. Rev. B (to be published).
[8]G. D. Mahan, *Many-Particle Physics*, (Plenum, New York, 1981).
[9]E. A. Taft and H. R. Philipp, Phys. Rev. **138**, A197 (1965). See also Ref. 13 of Ref. 7.
[10]G. D. Mahan, Phys. Rev. **153**, 882 (1967).
[11]J. M. Zhang, D. M. Hoffman, and P. C. Eklund (unpublished).

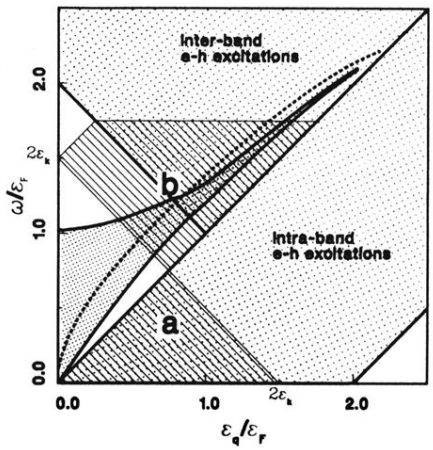

FIG. 2. The excitation spectrum of the system is shown by the dotted regions, which include both the electron-hole excitations (as indicated) and the plasmons (shown by the densely dotted band). Also shown is the 2D plasmon curve (the dashed curve) for a single graphite layer. Line-shaded regions demonstrate possible deexcitations for a conduction electron with the energy $\varepsilon_k = 0.75\varepsilon_F$. The regions denoted by a and b correspond, respectively, to the intraband process and the interband process. Only the deexcitations in the regions that overlap with the electron-excitation spectrum are actually allowed. It is obvious from this figure that only through interband processes can an electron decay into a plasmon.